05,13

Pecularities of magnetic textures in periodical multilayered Co/Pt films

© D.A. Tatarskiy[1,2], N.S. Gusev[1,2], O.L. Ermolaeva[1], A.N. Orlova[1], V.L. Mironov[1], S.A. Gusev[1]

[1] Institute of Physics of Microstructures, Russian Academy of Sciences,
Nizhny Novgorod, Russia
[2] Lobachevsky State University,
Nizhny Novgorod, Russia

E-mail: tatarsky@ipmras.ru

Received April 17, 2023
Revised April 17, 2023
Accepted May 11, 2023

The results of systematic experimental studies of the magnetic state and crystal structure of multilayer films based on a ferromagnet/heavy metal pair (Co/Pt) by optical magnetometry, magnetic force microscopy, Lorentz and analytical transmission electron microscopy are presented. It is shown that with an increase in the number of Co/Pt periods in the films, an increase in the average size of crystal grains is observed, which leads to an increase in the dispersion of perpendicular anisotropy and, as a consequence, to a decrease in the size of magnetic domains and magnetization reversal fields. In addition, in films with $n \geq 6$ periods, the domain wall becomes hybrid; has an intermediate structure between the walls of the Neel and Bloch types.

Keywords: Neel domain wall, cobalt-platinum, Dzyaloshinskii–Moriya interaction, Lorentz transmission electron microscopy, magnetic force microscopy.

DOI: 10.61011/PSS.2023.07.56405.40H

1. Introduction

Currently, thin-film structures based on ferromagnet/heavy metal (F/M) pair are extensively studied due to the possibility of stabilization of monochiral magnetic textures: Neel skyrmions, 360° domain walls, skyrmioniums, etc [1]. Stabilization mechanism is Dzyaloshinskii–Moriya interaction (DMI) on F/M interface occurring due to the absence of mirror symmetry σ_h in multilayer films [2]. The main methods of domain structure investigation in such films include the Lorentz transmission electron microscopy [3,4] and magnetic force microscopy [4–6].

In case of epitaxial multilayer structures, F/M and M/F interfaces are identical and the influence of surface DMI at these interfaces is cancelled [7]. However, polycrystalline multilayer periodic F/M structures demonstrate significant DMI despite the symmetric interfaces [8–10]. Moreover, the polycrystalline film structure imposes considerable influence on the random anisotropy [11–13], which affects the stabilization conditions of magnetic skyrmions [14].

The study contains the results of systematic investigations of magnetic state and crystalline structure of multilayer films based on Co/Pt pair by optical magnetometry (OM), magnetic force microscopy (MFM), Lorentz and analytical transmission electron microscopy (LTEM and ATEM, respectively) depending on the number of periods in the multilayer F/M structure.

2. Samples and methods

Thin-film Co/Pt structures were made by the magnetron sputtering method in argon atmosphere (pressure $4 \cdot 10^{-3}$ Torr) at room temperature. Multilayer structures were grown by sequential sputtering of Co, Pt and Ta targets. The average deposition rate was ~ 0.2 nm/s. Si(100) wafers and free-standing silicon nitride membranes of 30 nm thickness were used with Ta(2)Pt(4) buffer layers. Layer thicknesses in nanometers are specified in brackets hereinafter for each element. Multilayer $[\mathrm{Co}(0.5)/\mathrm{Pt}(1)]\times n$ structures were deposited on the substrates with buffer layers, where n is the number of periods in the structure. For the purpose of investigations, a set of samples with the number of periods $n = 2-18$ was prepared.

Magnetic properties of films were controlled by optical magnetometry methods by measuring magneto-optic Kerr effect (MOKE) in polar geometry at 632 nm (the bench was developed by Institute for Physics of Microstructures Russian Academy of Sciences). Domain magnetization structure was investigated using „Solver Pro“ (NT-MDT Spectrum Instruments, Zelenograd) magnetic-force microscope and „LIBRA 200 MC“ (Carl Zeiss, Jena) transmission electron microscope.

Standard NSG-1 cantilevers with magnetic coating were used as MFM sensors. Oscillation phase shift of the magnetic cantilever under the effect of force gradient from the stray fields of the sample was used as the MFM signal.

When the magnetic structure was investigated by the Lorentz transmission electron microscopy method, micro-images were recorded by the Fresnel method (defocusing method). The samples were placed in an analytical double tilt gatan specimen holder. Currents in the objective lens were set such that to compensate the magnetic field induced by the lens coils in the sample plane [15].

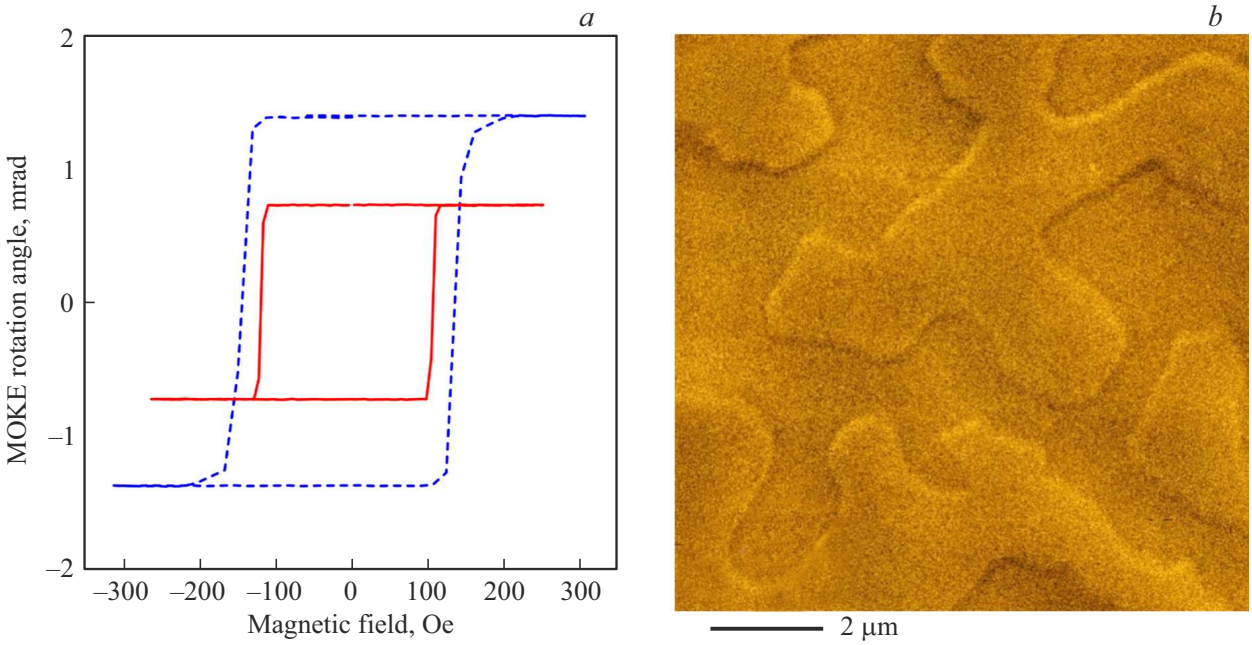

Figure 1. (*a*) MOKE magnetization loops of Co/Pt structures. A loop for [Co/Pt] × 2 film is shown by solid (red) line, for [Co/Pt] × 4 film is shown by dashed (blue) line. (*b*) MFM image of domain structure of [Co/Pt]×4 sample in demagnetized state.

Film crystallite sizes were defined using ATEM autocorrelation analysis of the microphotographs made in the dark field mode. The type of crystalline structure was defined by electron diffraction pattern rings obtained in the microdiffraction mode.

3. Results and discussion

According to OM investigations, all prepared samples had „easy axis“ type magnetic anisotropy oriented normally to the surface. The size of magnetic domains in demagnetized state was an important characteristic of magnetic properties of multilayer Co/Pt structures. Domain structure of the films was studied by the MFM and LTEM methods. Before the measurements, the samples were demagnetized by multiple remagnetization in a decaying magnetic field.

Ultrathin films with low number of periods ($n = 2, 3$) have distinctive perpendicular anisotropy and a rectangular MOKE loop with sharp transitions between the states with homogeneous magnetization. Figure 1, *a* shows magnetization loops for films with $n = 2$ and $n = 4$ for comparison. It can be seen that thin [Co/Pt]×2 film (Figure 1, solid red line) has almost a square loop, while the magnetization curve of [Co/Pt]×4 film (Figure 1, dashed line) has a small inclined section in the saturation attainment regions. Domain structure of [Co/Pt]×4 film in demagnetized state is shown in Figure 1, *b*. The average size of domains is equal to 1.5 μm.

With an increase in the number of periods ($n > 4$) in the Co/Pt structure on the magnetization loop, inclined sections increase and MOKE response grows. Figure 2, *a* shows as an example typical normalized MOKE loops for the samples with $n = 8$ and $n = 16$. In demagnetized state, these samples demonstrate a developed labyrinth domain structure. Typical LTEM and MFM images for the sample with $n = 8$ are shown in Figure 2, *b* and *c*, respectively. Average lateral sizes of magnetic domains were defined as half correlation quasiperiod in autocorrelation function for each MFM image. As an example, Figure 2, *d* shows autocorrelation function of the MFM image for [Co/Pt]×8 structure. It can be seen that the correlation quasiperiod for this domain structure is equal to 0.64 μm and, thus, the average domain size is 0.32 μm.

Important characteristics for samples with $n > 2$ include the dependences of demagnetization start fields H_{dem} and saturation field H_{sat} (shown in Figure 2, *a*), as well as average domain size on the number of periods *n*. Figure 3, *a* shows dependences $H_{dem}(n)$ and $H_{sat}(n)$. As shown in the figure, $n = 2$ H_{dem} and H_{sat} are almost coincide with each other. With the growing *n*, the saturation field increases monotonously from 100 Oe (for $n = 2$) to 2000 Oe (for $n = 18$), at the same time, the remagnetization field decreases and becomes negative for $n > 14$.

Dependence of the average domain size on the number of periods *n* is shown in Figure 3, *b*. It can be seen that the number of domains decreases sharply in the range $n = 2–8$, and then, for $n > 14$, remains almost constant.

According to the ATEM investigations, the increasing number of periods is accompanied with the increasing crystal grain sizes in the films. As an example, Figure 4, *a* shows a dark-field microphotograph of a [Co/Pt]×8 film segment. According to the microdiffraction data, all films

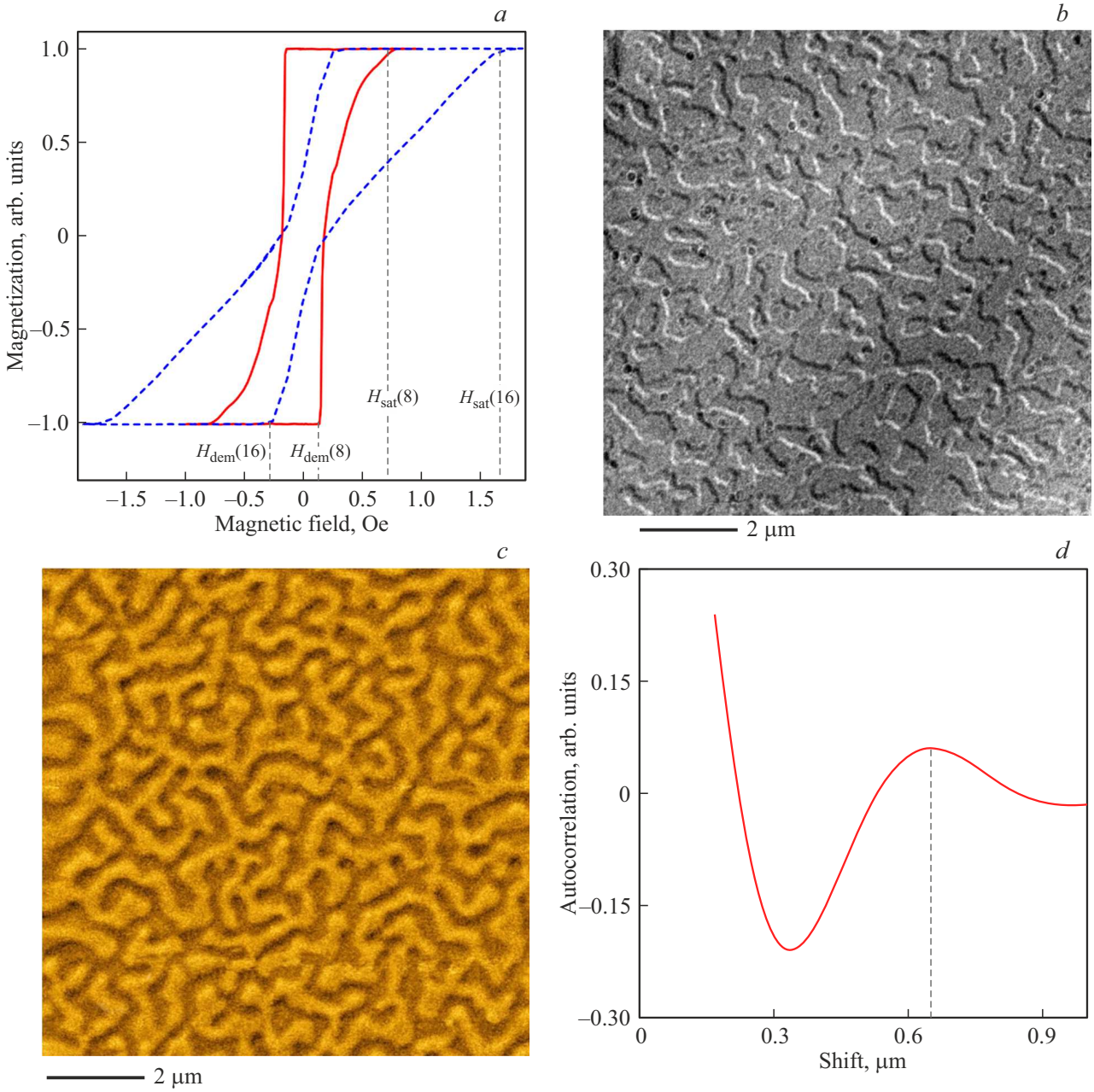

Figure 2. (*a*) MOKE magnetization loops for [Co/Pt]×8 (solid red line) and [Co/Pt]×16 structures (dashed blue line). Thin dashed lines show the saturation and magnetization fields. LTEM (*b*) and MFM (*c*) images of the domain structure of [Co/Pt]×8 film in the demagnetized state. (*d*) Autocorrelation function of MFM image of [Co/Pt]×8 film.

have a spatial symmetry group Fm3m with lattice constanct $a = 0.379 \pm 0.002$ nm. The films have a weak axial texture (111), which is defined by a significant decrease in intensity of the corresponding (smallest) diffraction ring (Figure 4, *a*).

The typical average crystal grain size in the films was defined by the width (at half maximum) of the autocorrelation function of the ATEM images. Whilst the obtained width shall be multiplied by 1.234 to obtain correct estimate of grain sizes [16]. The autocorrelation function section of the dark-field image of [Co/Pt]×8 sample is shown in Figure 4, *b*. As can be seen, the average grain size for this sample is 6.25 nm. Dependence of the average grain size on the number of periods in [Co/Pt]×*n* films is shown in Figure 3, *a*.

The increasing length of the inclined segment ($H_{sat}-H_{dem}$) and decreasing filed H_{dem} on the remagnetization loops with the growing number of layers are caused by the effect of two factors. On the one hand, with the growing *n*, the magnetostatic interaction effect increases resulting in the decreasing effective perpendicular magnetic anisotropy [17] and decreasing field H_{dem}. On the other

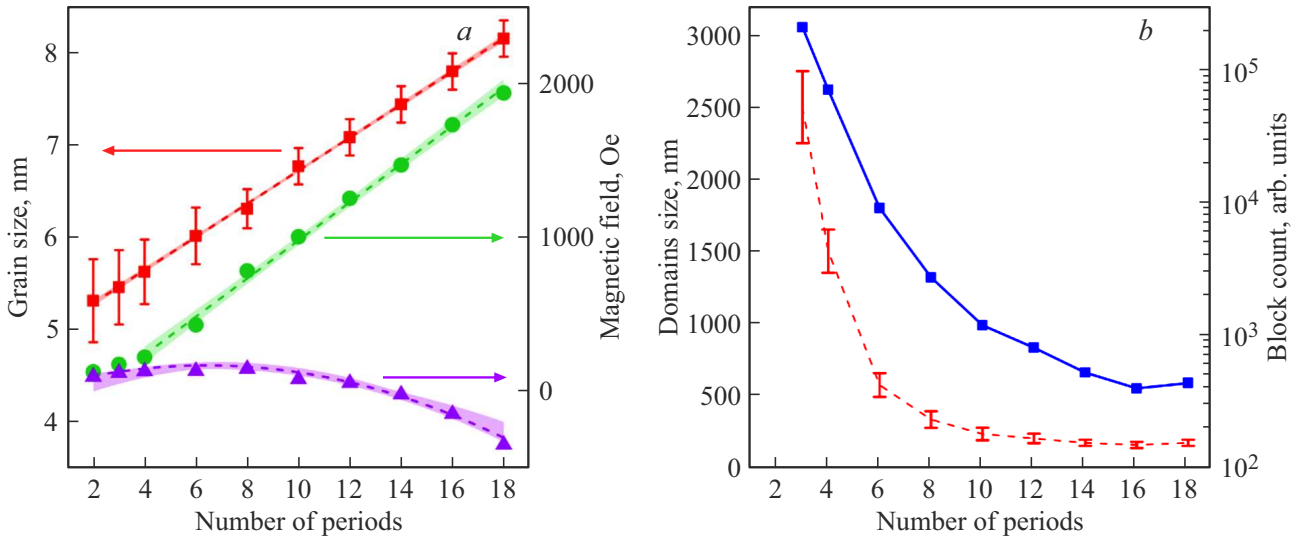

Figure 3. (*a*) The dependences of saturation field (green curve, circles), remagnetization field (purple curve, triangles) and average crystal grain size (red curve, squares) on the number of periods n in [Co/Pt]$\times n$ structure. (*b*) Dependences of the average lateral dimension of magnetic domains (red dashed line) and the average number of crystal blocks in one domain in the demagnetized state (blue line, squares) on the number of periods n in [Co/Pt]$\times n$ structure.

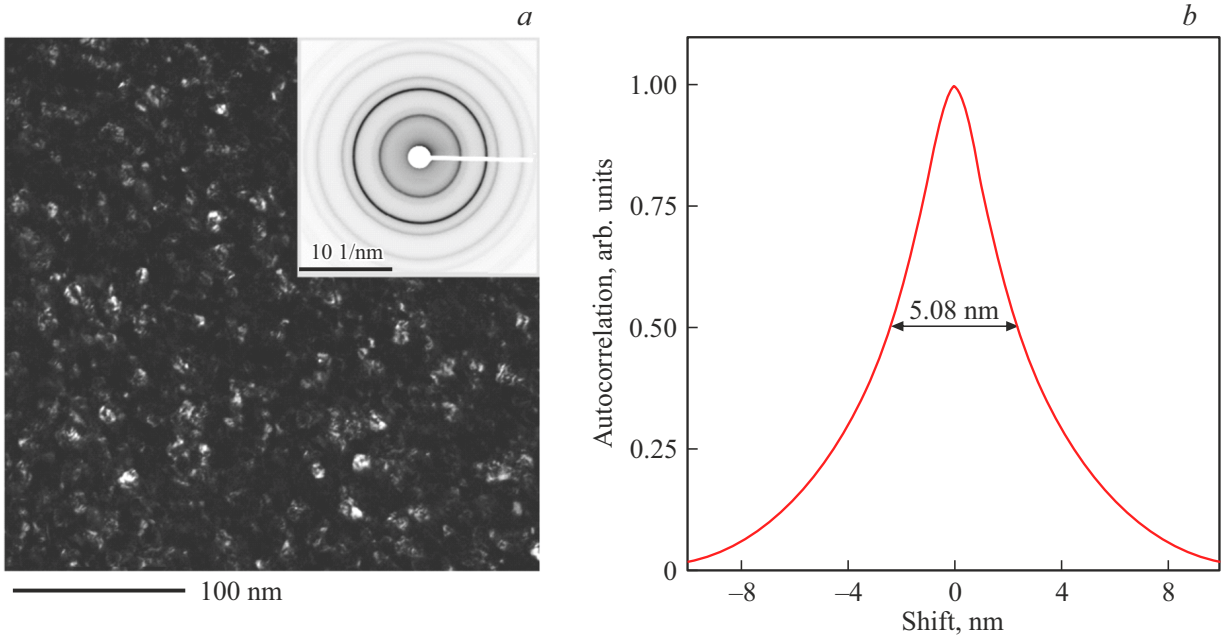

Figure 4. (*a*) Dark-field microphotograph of [Co/Pt]$\times$8 film. The detail shows typical microdiffraction rings. (*b*) Autocorrelation function corresponding to the microphotograph.

hand, with the growing n, the crystal grain size increases resulting in the increasing dispersion of the effective uniaxial anisotropy. Actually, the anisotropy dispersion is defined by the relation between the grain size and domain size, i.e. the number of grains in one domain. The average number of grains in one domain is estimated to decrease by three orders of magnitude with the varying number of periods in the range $n = 2-18$ (Figure 3, *b*). This is associated both with the growing grain size and decreasing average size of magnetic domains. Whilst the field H_{sat} is defined by the domains where the random anisotropy is such that their remagnetization may only occur in strong fields.

The change in the type of domain wall depending on the number of periods is another feature of [Co/Pt]$\times n$ structures. DMI are known to stabilize the Neel type domain wall [2]. However, in [Co/Pt]$\times n$ films, DMI is associated with exclusively interfacial interaction of cobalt

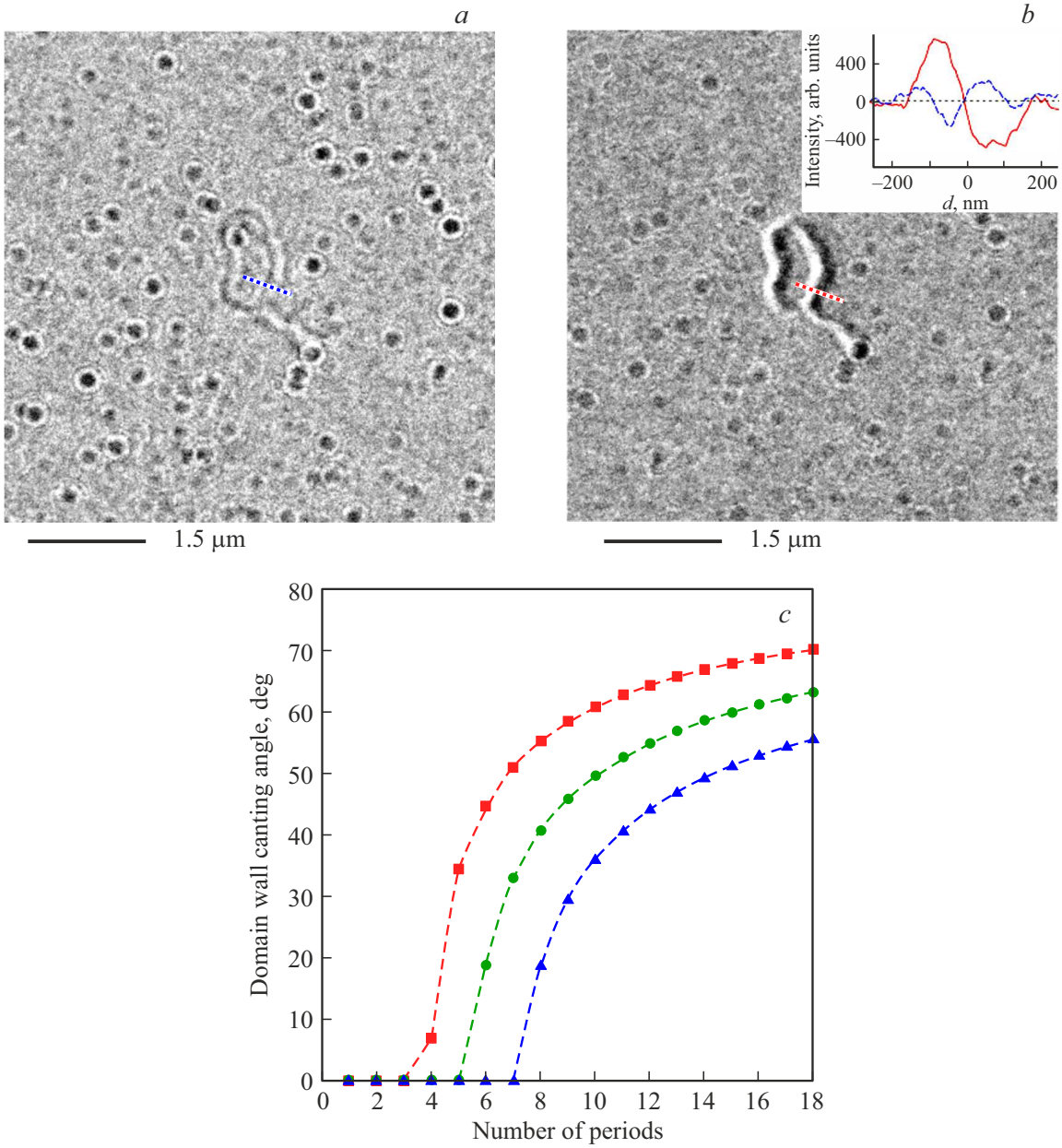

Figure 5. (a) LTEM image of the ring domain of [Co/Pt]×8 film with normal incidence of electronic beam. (b) LTEM image of the same ring domain with inclined sample. The detail shows distributions of contrast in the domain wall section along the axis of rotation of the sample (Figure 5, a — blue and 5, b — red dashed lines); (c) magnetization canting angle in the domain wall depending on the number of periods in the film at various DMI values: red squares — $D = 0.6\,\text{mJ/m}^2$, green circles — $D = 0.8\,\text{mJ/m}^2$, blue triangles — $D = 1.0\,\text{mJ/m}^2$.

atoms at the platinum interface [18]. With the growing number of n layers, contribution to the magnetostatic system energy increases from the bulk magnetostatic charges of the domain wall. As a result, for minimization of the magnetostatic energy, the domain wall becomes hybrid, i. e. has an intermediate structure between the Neel and Bloch type walls.

The effects of magnetostatic interaction and uniaxial anisotropy on the magnetization structure in the domain wall region may be estimated. Inclination angle γ of the domain wall from the Neel type wall is defined by the following relation [17]:

$$\begin{aligned} \cos\gamma &= \frac{\pi|D|}{k\Omega} \quad \text{for} \quad \pi|D| < k\Omega, \\ \gamma &= 0,\ \pi \quad \text{for} \quad \pi|D| < k\Omega, \end{aligned} \tag{1}$$

where D is the Dzyaloshinski–Moriya interaction constant, $\Omega = \mu_0 M_s^2$ (M_s is the saturation magnetization, μ_0 is the vacuum permeability), $k(t/\delta)$ is the function taking into account the magnetostatic interaction [18] (t is the film

thickness, δ is the domain wall thickness). For the estimates, the following constitutive parameters were used: exchange stiffness $A = 13 \cdot 10^{-12}$ J/m, $M_s = 10^6$ A/m, $\delta \approx 4.55$ nm In case when the numerator in (1) is higher than the denominator (DMI is much higher than the magnetostatic interaction), then this equation has no solutions and domain walls are of pure Neel type ($\gamma = 0$). Otherwise, the angle γ is calculated from the right-hand side of (1). Calculation results for the angle γ as a function of the number of periods in structure n for various DMI values are shown in Figure 5, *c*.

According to the LTEM investigations, the domain wall for $n \leq 4$ has the Neel structure and beginning from $n = 6$ the wall becomes hybrid. The type of domain wall was determined by the review of LTEM images of individual circular domains which are formed in the samples in the nearly saturated external magnetic field. Figure 5 shows typical LTEM images of the circular domain with 360° domain wall of $[Co/Pt]\times 8$ sample. The image in Figure 5, *a* has been recorded at the normal electron beam incidence and the image in Figure 5, *b* — at the inclined electron beam incidence. Distributions of the Fresnel contrast intensity along the line across the domain wall are shown in the inset (Figure 5, *b*). The illustrations show that the domain wall is of hybrid type. Contrast distribution corresponding to Figure 5, *a* is typical for the Bloch wall, while the distribution corresponding to Figure 5, *b* is specific for the Neel type domain wall. With the growing number of layers, the Bloch contrast intensity from the domain wall increases indicating its further hybridization. This allows to estimate DMI in $[Co(0.5)/Pt(1)]\times n$ structures. Diagram (Figure 5, *c*) shows that the transition from the Neel wall to the hybrid wall in this range n occurs for DMI values in the range $D = 0.6-1.0$ mJ/m^2 that agrees closely with D measured by the BLS methods for Co/Pt structures [19,20].

4. Conclusion

Thus, we had performed OM, MFM, LTEM and ATEM investigations of the crystal structure, magnetic state and domain wall configuration in multilayer thin-film $Ta(2)Pt(4)[Co(0.5)/Pt(1)]\times n$ samples depending on the number of periods n. It has been found that these samples are polycrystalline films with face-centered cubic lattice and have a weak axial texture (111), where an increase in the average crystal grain sizes is observed with the growing n. In the demagnetized state, the films are characterized by the labyrinth domain structure. With the growing number of periods n, a decrease in the magnetic domain sizes is observed. In addition, it has been shown that in the films with a low number of periods ($n \leq 4$), the Neel type domain wall is implemented, while in the films with a large number of periods ($n > 4$), hybrid domain wall is formed where a magnetization structure, which is intermediate between the Neel and Bloch wall structures, appears.

With the increasing number of layers, such factors as the Dzyaloshinskii–Moriya interfacial interaction, interlayer magnetostatic interaction and crystal grain growth result in decreasing effective uniaxial perpendicular anisotropy and, therefore, to the observed variation of remagnetization and saturation fields.

Acknowledgments

The authors would like to express their gratitude to M.V. Sapozhnikov and A.A. Fraerman for the helpful discussions.

Funding

This study was carried out under the state assignment of the Institute of Applied Physics, Russian Academy of Sciences (project 0030-2021-0021). Equipment provided by the „Physics and Technology of Micro- and Nanostructures“ CUC (Institute of Physics of Microstructures, Russian Academy of Sciences) was used for the study.

Conflict of interest

The authors declare that they have no conflict of interest.

References

[1] L. Wang, C. Liu, N. Mehmood, G. Han, Y. Wang, X. Xu, C. Feng, Z. Hou, Y. Peng, X. Gao, G. Yu. ACS Appl. Mater. Interfaces **11**, 12098 (2019).
[2] A.N. Bogdanov, D.A. Yablonsky. ZhETF **95**, 178 (1989). (in Russian).
[3] L. Peng, Y. Zhang, S. Zuo, M. He, J. Cai, S. Wang, H. Wei, J. Li, T. Zhao, B. Shen. Chin. Phys. B **27**, 066802 (2018).
[4] S. Zhang, J. Zhang, Y. Wen, E. Chudnovsky, X. Zhang. Nat. Comms. Phys. *1*, 36 (2018).
[5] A. Casiraghi, H. Corte-León, M. Vafaee, F. Garcia-Sanchez, G. Durin, M. Pasquale, G. Jakob, M. Kläui, O. Kazakova. Comms. Phys. **2**, 145 (2019).
[6] M.V. Sapozhnikov, N.S. Gusev, S.A. Gusev, D.A. Tatarskiy, Yu.V. Petrov, A.G. Temiryazev, A.A. Fraerman. Phys. Rev. B **103**, 054429 (2021).
[7] A. Hrabec, K. Shahbazi, T. Moore, E. Martinez, C. Marrows. Nanotechnology **30**, 234003 (2019).
[8] S.D. Pollard, J.A. Garlow, J. Yu, Z. Wang, Y. Zhu, H. Yang. Nat. Comms. **8**, 14761 (2017).
[9] J.A. Garlow, S.D. Pollard, M. Beleggia, T. Dutta, H. Yang, Y. Zhu. Phys. Rev. Lett. **122**, 237201 (2019).
[10] M.V. Dorokhin, A.V. Zdoroveyshchev, M.P. Temiryazeva, A.G. Temiryazev, P.B. Demina, O.V. Vikhrova, A.V. Kudrin, I.L. Kalentyeva, M.V. Ved, A.N. Orlova, V.N. Trushin, A.V. Sadovnikov, D.A. Tatarskiy. J. Alloys Comp. **926**, 166956 (2022).
[11] E.M. Chudnovsky, W.M. Saslow, R.A. Serota. Phys. Rev. B **33**, 251 (1986).
[12] G. Herzer. IEEE Transact. Magn. **26**, P. 1397 (1990).
[13] S.A. Gusev, D.A. Tatarsky, A.Yu. Klimov, V.V. Rogov, E.V. Skorokhodov, M.V. Sapozhnikov, B.A. Gribkov, I.M. Nefedov, A.A. Fraerman. FTT, **55**, 435 (2013). (in Russian).

[14] E.M. Chudnovsky, D.A. Garanin. New J. Phys. **20**, 033006 (2018).
[15] D.A. Tatarsky, N.S. Gusev, S.A. Gusev. Ultramicroscopy (2023). In press.
[16] B. Zang, K. Suzuki, A. Liu. Mater. Characterization **142**, 577 (2018).
[17] T.N.G. Meier, M. Kronseder, C.H. Back. Phys. Rev. B **96**, 144408 (2017).
[18] H. Yang, A. Thiaville, S. Rohart, A. Fert, M. Chshiev. Phys. Rev. Lett. **115**, 267210 (2015).
[19] N.S. Gusev, Yu.A. Dudin, A.V. Sadovnikov, M.V. Sapozhnikov. FTT, **63**, 1263 (2021). (in Russian).
[20] M.V. Sapozhnikov, R.V. Gorev, E.V. Skorokhodov, N.S. Gusev, A.V. Sadovnikov, O.G. Udalov. Phys. Rev. B **105**, 024405 (2022).

Translated by Ego Translating